Title: Bursting emerges from the complementary roles of neurons in a four-cell network

Running Head: Dynamic properties within a half-center oscillator

Authors: Akira Sakurai[1]* and Paul S. Katz[2]

1. Neuroscience Institute, Georgia State University, Atlanta, GA 30302-5030, USA

2. Department of Biology, University of Massachusetts Amherst, Amherst MA 01003, USA

*Corresponding author, Neuroscience Institute, Georgia State University, Atlanta, GA 30302-5030, USA akira@gsu.edu

Number of pages: 24

Number of Figures: 11

Number of Tables: 0

Number of Words:

Abstract: 240

Introduction: 371

Discussion: 1789

Conflict of interest: The authors declare no competing financial interests.

Acknowledgments: This work was supported by NSF grant IOS-1120950.

Abstract (240/250 words)

Reciprocally inhibitory modules that form half-center oscillators require mechanisms for escaping or being released from inhibition. The central pattern generator (CPG) underlying swimming by the nudibranch mollusc, *Dendronotus iris*, is composed of only four neurons that are organized into two competing modules of a half center oscillator. In this system, bursting activity in left-right alternation is not driven by any of the neurons but is an emergent property of the network as a whole. We found that the unique synaptic actions and membrane properties of the two neurons in each module (Si2 and Si3) play complementary roles in generating stable bursting in this network oscillator. Only Si2 evokes fast and strong inhibition of its contralateral counterpart, the termination of which initiates post-inhibitory rebound in the Si3 of that module. Only Si3 is responsible for the rebound excitation because it has a hyperpolarization-activated inward current. Within each module, the synaptic actions and membrane properties of the two neurons complement each other: Si3 excites Si2, which then feeds back slow inhibition to Si3, terminating the burst. Using dynamic clamp, we showed that the magnitude of the slow inhibition sets the period of the oscillator. Thus, the synaptic actions of Si2 provide the hyperpolarization needed for the other module to rebound stably, whereas the membrane properties of Si3 in each module cause it to rebound first and excite Si2 and maintain the burst until the cycle repeats and the other module becomes active.

Key words: Rhythmogenesis; Gastropod; Locomotion; voltage clamp, Invertebrate

Introduction

Since the original proposal of the half-center oscillator (HCO) concept by Brown (1911), reciprocal inhibition between two modules has been considered to be the fundamental architecture of network oscillators (Grillner and El Manira 2015; Kiehn 2016; Moult et al. 2013). However, reciprocal inhibition by itself is not sufficient to maintain stable rhythmic bursting. In many systems, endogenous or conditional bursting properties contribute to maintaining the alternation of half-center oscillators (Arshavsky et al. 1986; Cymbalyuk et al. 2002; Kiehn et al. 1996; Li et al. 2010; Reith and Sillar 1998; Selverston and Miller 1980; Wallen and Grillner 1987). A mechanistic cellular-level understanding of network-driven oscillations in a central pattern generator (CPG) has been difficult to determine because of the large numbers of neurons in most network oscillators. The CPG underlying swimming in the nudibranch mollusc, *Dendronotus iris* is a network oscillator consisting of only four neurons (Sakurai and Katz 2016). Here we examined synaptic actions and membrane properties of these two pairs of bilaterally represented neurons in the generation of stable bursting activity.

Dendronotus swims by rhythmically flexing its body in alternation from left to right (Sakurai et al. 2011). The rhythmic motor pattern originates from a swim CPG that consists of neurons swim interneurons numbered Si2 and Si3 (Fig. 1A,B) (Sakurai and Katz 2016). Both Si2 and Si3 reciprocally inhibit their contralateral counterparts contributing to the left-right alternation (Fig. 1B). However, the two modules of the HCO, which we label α and β here, consist of the contralateral Si2 and Si3, such that the left Si2 and the right Si3 fire in phase with each other as module α and the right Si2 fires with the left Si3 as module β (Fig. 1C*i*). A strong excitatory synapse from Si3 to the contralateral Si2 and electrical coupling between the pair mediates their synchronous firing in each module (Fig. 1C*ii*). In this study, we investigated the mechanisms underlying the transition of activity between the two modules of the swim CPG. We found that each of the two neurons in a module contributes differently to burst initiation and termination of the cycle. Specifically, the combined action of a slow synapse and active membrane properties provide dynamic features needed for this half-center oscillator to function.

72

73 **Materials and Methods**

74 *Animal collection, maintenance, and dissection*

75 Specimens of *Dendronotus iris* (Mollusca; Gastropoda; Nudibranchia), 6-20 cm long,
76 were collected on the Pacific coast of North America by Monterey Abalone Company
77 (Monterey, CA) and Living Elements Ltd (Delta, BC, Canada). The animals were kept in artificial
78 seawater tanks at 10-12°C with a 12:12 light/dark cycle.

79 Before the surgery for brain isolation, the animal was anesthetized by injecting 0.33 M
80 magnesium chloride solution (20-50 mL) into the body cavity, and an incision was made
81 through the body wall near the esophagus. Then all nerve roots exiting the brain were severed,
82 and the brain (Fig. 1A) was isolated by severing the esophagus. The isolated brain was pinned
83 with the dorsal side up on the bottom of a Sylgard-lined dish and perfused at a rate of 0.5
84 ml/min with normal saline (mM: 420 NaCl, 10 KCl, 10 $CaCl_2$, 50 $MgCl_2$, 11 D-glucose, 10 HEPES,
85 pH 7.6) or artificial seawater (Instant Ocean, Mentor, OH). The brain was chilled down to 4°C,
86 and the connective tissue and the brain sheath were removed with forceps and fine scissors.
87 After desheathing, the temperature was raised to 10°C for electrophysiological experiments.

88 *Electrophysiology*

89 Intracellular recordings were performed using 15-35 MΩ glass microelectrodes filled with a
90 solution containing 2 M potassium acetate and 0.2 M potassium. Each electrode was connected
91 to the headstage of Axoclamp 2B amplifier (Molecular Devices, Sunnyvale, CA). The output
92 signals of the amplifier were digitized at a sampling frequency of >2 kHz using a 1401Plus or
93 Micro1401 A/D converter (Cambridge Electronic Design, Cambridge, UK). Data acquisition and
94 analysis were performed with Spike2 software (CED, Cambridge, UK) and SigmaPlot (Jandel
95 Scientific, San Rafael, CA).

96 To investigate the effects of depolarization or hyperpolarization of the swim
97 interneurons on the swim rhythm, a positive or negative current pulse (from -4 nA to 4 nA) was

injected directly into the neurons via bridge-balanced microelectrodes. To investigate monosynaptic connection between swimming interneurons, high-divalent cation (Hi-Di) saline was applied to raise the spike threshold and suppress spontaneous neural firing. The composition of Hi-Di saline (in mM) was 285 NaCl, 10 KCl, 25 $CaCl_2$, 125 $MgCl_2$, 11 D-glucose, 10 HEPES, pH 7.6. To measure the reversal potentials of synaptic potential or synapticc current, the membrane potential was manipulated by injecting a steady current through an additional microelectrode placed in the same neuron. In some experiments, calcium-free Hi-Di saline was used to block chemical synaptic transmission. In low calcium Hi-Di saline, $CaCl_2$ was replaced by $MgCl_2$.

Dynamic clamp

To artificially enhance or counteract the Si2-evoked slow IPSPs in Si3, we performed dynamic clamping with the software StdpC (Kemenes et al. 2011) as described previously (Sakurai and Katz 2017; 2016; 2019; Sakurai et al. 2014b). Each Si3 was impaled with two microelectrodes, one for membrane potential recording and the other for current injection (see Fig. 10Ai). Every time Si2 generated an action potential that exceeded 0 mV, the current injected into the postsynaptic Si3, I_{stim}, was calculated using a first order kinetics model of the release of neurotransmitter (Destexhe et al. 1994; Kemenes et al. 2011; Sharp et al. 1996):

$$I_{\mathrm{syn}} = g_{\mathrm{syn}}\, S(t)[V_{\mathrm{syn}} - V_{\mathrm{post}}(t)], \qquad \text{(eq. 1)}$$

where $S(t)$ is the instantaneous synaptic activation, g_{syn} is the maximum synaptic conductance, V_{syn} is the reversal potential (-70 mV) of the synapse. To counteract Si2-evoked synaptic potentials, a negative value was used for g_{syn}.

The instantaneous activation, $S(t)$ is given by the differential equation:

$$\left(1 - S_{\infty}\left(V_{\text{pre}}\right)\right)\tau_{\text{syn}}\frac{dS}{dt} = \left(S_{\infty}\left(V_{\text{pre}}\right) - S(t)\right), \qquad \text{(eq. 2)}$$

where

$$S_{\infty}\left(V_{\text{pre}}\right) = \begin{cases} \tanh\left[\frac{V_{pre} - V_{thresh}}{V_{slope}}\right] & if\ V_{pre} > V_{Thresh} \\ 0 & otherwise \end{cases} \qquad \text{(eq. 3)}$$

S_{∞} is the steady state synaptic activation and τ_{syn} is the time constant for synaptic decay. The time constant of the falling phase of the Si2-evoked slow IPSC in Si3 was 0.94 ± 0.2 sec (N = 5). In this study, τ_{syn} was set to 1.0 sec. V_{pre} is the presynaptic membrane potential of Si3 and V_{thresh} is the threshold potential for the release of neurotransmitter; it was set to the level of 50% height of the smallest Si3 action potentials. The synaptic slope parameter of the activation curve (V_{slope}) was set to 25 mV. g_{syn} was varied between -1000 and 1000 nS.

Statistics

Statistical comparisons were performed using SigmaPlot ver. 12.5 (Jandel Scientific, San Rafael, CA) for Student's *t*-test, paired *t*-test, and Kruskal-Wallis one-way ANOVA on Ranks with all pairwise multiple Comparison Procedures. Shapiro-Wilk test was used to assume normality of data structure. In all cases, P<0.05 was considered significant. For *t*-tests, two-tailed P value was used. Results are expressed as the mean ± standard deviation (SD).

Results

Si2-evoked IPSPs had a more hyperpolarized reversal potential than those of Si3

In the *Dendronotus* swim CPG, two neurons, Si2 and Si3, each form inhibitory reciprocal synapses with their contralateral counterparts (Fig. 1B). When compared in high divalent cation

145 (Hi-Di) saline, which raises spike threshold, thereby minimizing spontaneous and polysynaptic
146 activity, the reversal potentials of the two synapses differed (Fig. 2). The average reversal
147 potential of Si2-to-SI2 IPSPs was -73.9 ± 8.1 mV (N = 5; Fig. 2A*i*, B), whereas the Si3-to-Si3 IPSP
148 reversal potential was -49.6 ± 6.5 mV (N = 6; Fig. 2A*ii*, B). There was a significant difference
149 between these values (P < 0.001 by two-tailed t-test), suggesting that the currents underlying
150 the IPSPs differ in ionic carriers. Thus, Si2 hyperpolarized its contralateral counterpart to a
151 much greater extent than Si3 did when the postsynaptic neurons were near their resting
152 potentials (about -50 mV).

153 *Si2 evoked a larger inhibitory effect on the opposite module than did Si3.*

154 During each cycle of the swim motor pattern, both Si2 and Si3 receive prolonged synaptic
155 inhibition from their contralateral counterparts. To better evaluate the contributions of Si2 and
156 Si3, we mimicked the activity during the swim motor pattern by stimulating each neuron
157 independently with a 4 second train of action potentials (Fig. 3). When Si2 was stimulated, it
158 caused a brief hyperpolarization and a delayed depolarization in both the Si2 and Si3 of the
159 opposite module, which led to a post-inhibitory rebound (PIR) burst of action potentials in Si3
160 (Fig 3A). In 68% of those preparations (N=19 of 28), the contralateral Si2 also showed a PIR
161 discharge, however, these were all triggered by the Si3-evoked EPSPs (Fig. 3A, asterisks). Thus,
162 the inhibitory synaptic inputs from Si2 not only provided inhibition to the other half-center
163 module, but they also induced an excitatory response in Si3 *via* PIR excitation.

164 In contrast, when Si3 was stimulated to produce a similar train of action potentials, as
165 expected by the less negative reversal potential, the inhibitory synaptic potentials generated in
166 Si2 and Si3 of the opposite module were markedly smaller than those generated by Si2 (Fig.
167 3B). Rebound firing in the contralateral Si3 occurred in only 69% of preparations (N=11 of 16),
168 which induced the ipsilateral Si2 firing in 43.8% of those preparations (N = 7 of 16). Thus, Si3
169 was less effective than Si2 in causing a rebound discharge of Si3 in the opposite module.

170 The difference in the size of the evoked inhibitory potentials in response to a train of
171 action potentials was more pronounced in Hi-Di saline (Fig. 4). A 4 sec, 10Hz spike train in Si2

172 hyperpolarized the contralateral Si2 by -11.7 ± 1.3 mV (N = 15, Fig. 4A,C). Si2 also
173 hyperpolarized the ipsilateral Si3 by -6.4 ± 1.5 mV (N=15, Fig. 4A,C), because it is electrically
174 coupled to the right Si2 (Sakurai and Katz 2016). In contrast, a 4 sec, 10 Hz spike train in Si3
175 hyperpolarized the contralateral Si3 by -2.2 ± 0.9 mV (N = 7) and the ipsilateral Si2 by -2.4 ± 1.0
176 mV (N = 9) (Fig. 4B,C). Thus, Si2 was more effective at inhibiting the other module than Si3 was.

177 *Si3, but not Si2, exhibited post-inhibitory rebound*

178 After cessation of an Si2 spike train, Si3 in the other module not only recovered more quickly
179 but also showed a PIR depolarization that exceeded above the original membrane, which was
180 absent in Si2 (Fig. 4A, asterisk). Neither neuron exhibited rebound depolarization when Si3 was
181 stimulated (Fig. 4B). The rebound depolarization induced by Si2 onto the Si3 in the other
182 module was significantly larger than any other synaptic combination (Fig. 4D, P<0.05 by Kruskal-
183 Wallis one-way ANOVA on Ranks with all pairwise multiple Comparison Procedures).

184 Si3 exhibited a larger PIR depolarization than Si2 following a hyperpolarizing current
185 step (Fig. 5). In normal saline, cessation of a hyperpolarizing current pulse (4 sec, 1-4 nA)
186 injected into Si2 produced few if any spike discharges (Fig. 5A*i*, B). In contrast, Si3 always
187 exhibited a PIR discharge upon termination of the pulse (Fig. 5A*ii*, B). The number of spikes
188 after the current pulse was significantly larger in Si3 than in Si2 (Fig. 5B; P < 0.001 by Two-way
189 repeated-measures ANOVA with Holm-Sidak method, N = 9-12 for Si2 and N = 8-10 for Si3).
190 With spike threshold elevated in Hi-Di saline, the membrane potential of Si2 quickly returned to
191 resting potential when released from the hyperpolarizing current injection (Fig. 5C*i*), whereas
192 Si3 showed a depolarizing overshoot (Fig. 5C*ii*, asterisk) that was significantly larger than seen
193 Si2 (Fig. 5D; P < 0.001 by Two-way repeated-measures ANOVA with Holm-Sidak method, N = 20-
194 23 for Si2 and N = 19-21 for Si3).

195 *Si3, but not Si2, exhibited a hyperpolarization-activated inward current*

196 Si3 exhibited a larger "sag" potential than Si2 in which the membrane potential
197 gradually depolarized during sustained injection of hyperpolarizing currents greater than -3nA
198 (Fig. 5A, C, E; P < 0.001 by two-way repeated-measures ANOVA with Holm-Sidak method, N =

199 23 for Si2 and N = 21 for Si3). Under voltage clamp, Si3, but not Si2 exhibited a
200 hyperpolarization-activated inward current (Fig. 6). Hyperpolarizing command voltage steps did
201 not produce noticeable current response in Si2, whereas in Si3 they evoked slow inward
202 currents at potentials more negative than -70mV (Fig. 6). Thus, Si2 and Si3 had distinct
203 membrane properties; the hyperpolarization-activated slow inward current in Si3 likely
204 underlies the sag depolarization and subsequent rebound depolarization, which produces the
205 PIR discharge in Si3 and consequently induces the phase transition from one module of the half
206 center to the other.

207 *Si2 evoked a slow synaptic inhibitory potential in Si3 within each module*

208 We previously demonstrated that Si3 excites the Si2 in the same module through both a
209 strong chemical synapse and strong electrical coupling, causing them to fire in near synchrony
210 (Sakurai and Katz 2016). Here we found that Si2 inhibited Si3, causing it to stop firing action
211 potentials when stimulated with a train (Fig 7A).

212 When spike threshold was increased in Hi-Di saline, an Si2 spike train produced a one-
213 for-one electrotonic EPSPs in the contralateral Si3 (Fig. 7B*i*). With increased spike frequency, a
214 slowly increasing hyperpolarizing potential counteracted the electrotonic EPSPs and produced
215 an overall hyperpolarization (Fig. 7B*i*, 10 Hz). Application of Ca^{2+}-free saline blocked this
216 hyperpolarization without changing the electrotonic EPSPs (Fig. 7B*ii*, C). Subtracting traces in
217 Ca^{2+}-free saline (Fig. 7B*ii*) from those in Hi-Di saline (Fig. 7B*i*) revealed the Ca^{2+}-sensitive
218 component of the Si2-evoked postsynaptic potential in Si3 (Fig. 7B*iii*). Thus, Si2 was electrically
219 coupled to Si3 and inhibited it through a slow potential caused by neurotransmitter release.

220 When Si3 was voltage-clamped, a spike train in the contralateral Si2 produced a slowly
221 rising inhibitory postsynaptic current (IPSC) whose amplitude was outwardly rectifying (Fig.
222 8A,B). The reversal potential was variable across individuals ranging from -60 to -80 mV (Fig.
223 8B). The time constant of the falling phase of the slow IPSC was 0.94 ± 0.2 sec (N = 5). During
224 the Si2 spike train, the membrane conductance of Si3 increased in all three preparations
225 examined from an average of 80.7 ± 15.3 nS to 141 ± 22.1 nS (P = 0.039 by paired *t*-test, N = 3).

226 The outward rectification of the slow IPSC was not likely due to a change in background
227 membrane conductance via opening or closing of voltage-gated channels, because in the
228 absence of Si2 stimulation, the current/voltage relation was linear throughout the voltage
229 range examined (Fig. 8C). At present, it is unclear how such apparent outward rectification was
230 brought about; the variability in the reversal potential and the non-linearity of the I-V
231 relationships could also be an experimental artifact caused by poor space clamping, suggesting
232 that the site of synaptic input from Si2 is located contralateral to the Si3 soma.

233 *Feedback inhibition from Si2 to Si3 contributed to burst termination*

234 To determine the role that the inhibition from Si2 to the contralateral Si3 plays in
235 rhythmic bursting, we examined the effect of suppressing spikes in Si2 during the swim motor
236 pattern (Fig. 9). When unperturbed, the intra-burst spike frequency of Si3 showed an initial
237 peak and a subsequent steep decline during each burst (Fig. 9A,B, burst *a* - blue). Suppression
238 of spiking in the co-active Si2 by injection of hyperpolarizing current immediately increased the
239 duration of Si3 bursts (Fig. 9A,B burst *b* - red). The mean duration of Si3 bursts during the swim
240 motor pattern increased significantly from 2.7 ± 0.9 sec to 4.1 ± 1.1 sec when the Si2 in its
241 module was hyperpolarized to prevent it from spiking (Fig. 9C*i*; $P < 0.001$ by two-tailed paired t-
242 test, N=12). Suppressing Si2 firing significantly increased both the mean duty cycle of Si3 bursts
243 from 0.54 ± 0.09 to 0.67 ± 0.13 (Fig. 9C*ii*; $P < 0.001$ by Wilcoxon Signed Rank Test, N = 12) and
244 the mean number of Si3 spikes from 19.5 ± 4.9 to 28.4 ± 9.3 ($P < 0.001$ by two-tailed paired t-
245 test, N = 12) (Fig. 9C*iii*). Thus, although Si2 is electrically coupled to the Si3 in its module, the
246 main effect of Si2 was to slowly decrease Si3 firing through a chemical inhibitory synapse.

247 *The magnitude of the slow inhibition from Si2 to Si3 played a role in setting burst period.*

248 The results suggest that the slow inhibition from Si2 to Si3 in each module decreases Si3
249 firing and hence deceases the excitatory drive from Si3 to Si2. We hypothesized that the self-
250 inhibition within the module helps to terminate the burst and transition to activation of the
251 other module. To test this, we systematically enhanced or reduced the magnitude of the
252 inhibition from Si2 to Si3 in both modules during a swim motor pattern using the dynamic

253 clamp technique. The amplitudes and time courses of the Si2-evoked synaptic currents were
254 calculated in real time (see Materials and Methods) and injected into Si3 through the recording
255 electrode in response to spikes in the contralateral Si2 (Fig. 10A*i*). While the dynamic clamp was
256 engaged, an Si2 burst set off a slow negative current injected into Si3, boosting the slow
257 inhibitory synapse, which shortened the Si3 burst (Fig. 10A*ii*). Spikes in the postsynaptic Si3 also
258 produced spike-like downward surges in the injected current, because the spikes moved the
259 membrane potential away from the reversal potential of the slow IPSC (-70 mV), increasing the
260 driving force for the current.

261 Augmenting the amplitude of the Si2-to-Si3 slow inhibitory synaptic conductance
262 shortened the Si3 burst duration, thereby decreasing the burst period (Fig. 10B,D). In contrast,
263 counteracting the inhibition with an inverted conductance reduced the Si2-to-Si3 inhibition and
264 extended Si3 bursts, thereby increasing the burst period (Fig. 10C,D). Thus, the feedback
265 inhibition from Si2 to Si3 within each module plays a crucial role in maintaining the periodicity
266 of the half-center oscillator.

267

268 **Discussion**

269 The results presented show that stable alternating bursting in the *Dendronotus* swim CPG is an
270 emergent property of the network that arises from the synaptic actions and the membrane
271 properties of the four neurons, with the two neurons in each module playing complementary
272 roles in burst initiation and termination (Fig 11). Specifically, we found that synaptic inhibition
273 of Si2 by its contralateral counterpart in the opposite module provides the hyperpolarization
274 needed for the electrically-coupled Si3 to rebound and fire action potentials. The spikes in Si3
275 then excite Si2 causing both neurons to fire a maintained train of spikes. Si2 spiking slowly
276 inhibits Si3, eventually terminating the burst and releasing the opposite module for the next
277 burst. This creates a sequence of activation and feedback inhibition in which each of the four
278 neurons in turn becomes dominant (Fig. 11 B,C).

Feedback inhibition as a mechanism of release in a HCO

A key finding of this study is the discovery of a synaptic mechanism that serves as a brake on self-excitation within each module of the half-center circuit. In a previous study, we found that Si3 excites the Si2 in its module with very large EPSPs and the two neurons are tightly coupled by electrical synapses, causing synchronized activity that is essential for maintaining half-center oscillator activity (Sakurai and Katz 2016). Here, we found that Si2 evokes slow inhibitory potentials in Si3 that summate until Si3 stops firing, thereby ending the burst. The magnitude of this feedback inhibition sets the burst duration of the HCO as shown with dynamic clamp manipulation.

Previously, Friesen (1994) suggested that spike frequency adaptation of each half-center module or fatigue of mutually inhibitory synapses are the potential mechanisms that release the other module from inhibition. However, few such circuits have been reported; instead, neural circuits with a half-center configuration often are capable of generating endogenous bursting upon isolation (see however: Arshavsky et al. 1986; Cymbalyuk et al. 2002; Selverston and Miller 1980). To our knowledge there have been no prior reports of inhibition within a module playing an essential role in other HCOs. The division of labor between Si2 and Si3 within each module allows the summation of synaptic inhibition from Si2 to Si3 to serve as a mechanism that determines burst duration.

Distinct roles for contralateral inhibition

Although both Si2 and Si3 had reciprocal inhibitory synapses with their contralateral counterparts, as is typical for a half-center oscillator, only the Si2 synapses were responsible for triggering PIR in the opposite module. The Si2-Si2 IPSPs were larger than the Si3-Si3 IPSPs because they had a more negative reversal potential. The Si2 spike train hyperpolarized Si3 in the opposite module, but this action was indirect through electrical coupling from Si2 to Si3 within that module. The inhibitory effect of the Si3-evoked IPSPs was mostly due to shunting inhibition caused by an increase in membrane conductance because their reversal potential was close to the resting membrane potential (Paulus and Rothwell 2016).

306 The synaptic actions of Si2 and Si3 differed depending on the postsynaptic cell,
307 suggesting that the postsynaptic neurons differ in receptor type. The Si2-Si2 synaptic potentials
308 were rapid, with a reversal potential suggestive of a ligand-gated potassium channel. The Si2 to
309 Si3 synaptic potentials also had a reversal potential near potassium equilibrium, but the fact
310 that they did not appear as discrete synaptic potentials corresponding to the presynaptic spikes
311 and their slow kinetics suggests that they are mediated by a G-protein coupled receptor. The
312 Si3-Si3 synaptic properties are consistent with being mediated by a ligand-gated chloride
313 channel. The Si3-Si2 synapse appears to be mediated by a ligand gated cation channel with a
314 reversal potential estimated to be near 0 mV (Sakurai and Katz 2016). Both effects of Si3 are
315 blocked by curare (Sakurai and Katz 2017), suggesting that they are mediated by different
316 variant of nicotinic acetylcholine receptors, which can be cation or anion selective in molluscs
317 (Jiao et al. 2019; van Nierop et al. 2006; van Nierop et al. 2005).

318 *Different PIR properties for burst initiation*

319 Only the Si3 each module showed PIR when released from hyperpolarization or after a train
320 of IPSPs evoked by the other half-center module. The mechanism for the PIR was a
321 hyperpolarization-activated inward current, which was absent in Si2. This difference in
322 membrane properties ensures that Si3 fires before Si2 during each burst. This may contribute
323 to the stability of bursting by inserting a delay before feedback inhibition from Si2 can occur.

324 The sag potential that develops as a result of accumulation of the hyperpolarization-
325 activated inward current may contribute to the escape of these neurons from synaptic
326 inhibition from the opposing module as seen in other systems. (Arbas and Calabrese 1987;
327 Pirtle et al. 2010). Thus, the *Dendronotus* HCO has elements of both release and escape
328 mechanisms as suggested by the occasional overlap of the first Si3 spike and the last Si2 spike
329 of the opposite module (for example, Fig. 11B)

330 Active membrane properties of neurons, such as “sag” depolarization and PIR, have been
331 shown to be involved in the transition of activity by allowing the postsynaptic neurons to
332 escape from inhibition or firing once released from inhibition (Arbas and Calabrese 1987;

333 Arshavsky et al. 1985; Dethier et al. 2015; Li and Moult 2012). Studies using computer models
334 also demonstrated the role of PIR in escaping from inhibition (Daun et al. 2009; Perkel and
335 Mulloney 1974; Wang and Rinzel 1992). Here we found that one neuron in each module had
336 this function.

337 *The Dendronotus swim CPG is a true network oscillator*

338 Many neural circuits with a half-center configuration are capable of generating
339 endogenous bursts upon isolation of the two modules (Arshavsky et al. 1986; Cymbalyuk et al.
340 2002; Selverston and Miller 1980). Similarly, conditional pacemaker properties also have been
341 found in each half of the locomotor circuit in the spinal cord (Kiehn et al. 1996; Li et al. 2010;
342 Reith and Sillar 1998; Wallen and Grillner 1987). When the left and right modules of the spinal
343 swimming circuit are separated in lamprey, each module exhibits rhythmic bursting activity at a
344 faster rhythm than normal (Grillner 2003). If each half-center possesses endogenous
345 rhythmogenesis, then, the role of mutual inhibition between half-centers is limited to ensuring
346 coordinated bursts occur in alternation (Ausborn et al. 2018; Hagglund et al. 2013). A
347 counterexample to this was reported by Moult et al. (2013), in which they showed that the
348 onset of rhythmic activity did not occur instantaneously when unilateral activity is momentarily
349 inhibited, but took some time, suggesting that some neuroplasticity may be involved in the
350 experimentally induced onset of unilateral automaticity.

351 In *Dendronotus*, it is unlikely that each module of the swim CPG has rhythmogenesis
352 because no oscillatory activity was seen when the activity of one side was suppressed by
353 current injection (Sakurai and Katz 2016). Furthermore, blocking the synaptic actions Si3 with
354 curare halts all rhythmic activity (Sakurai and Katz 2017). The Si3 pair alone cannot generate
355 oscillatory activity even when depolarized by current injection. Thus, the *Dendronotus* swim
356 CPG is a unique example of a network oscillator with a half-center configuration, in which none
357 of the neurons, nor the opposite modules are capable of rhythmogenesis; rhythmic activity is
358 an emergent property of the network as a whole.

359 *All synaptic connectivity in the pedal ganglia is contralateral*

360 It is worth noting that almost all of the synapses made by pedal ganglion neurons in
361 both *Dendronotus* all other nudibranchs studied are between contralateral neurons; very few
362 synapses have ever been found between pedal ganglion neurons whose somata are ipsilateral
363 to each other (Sakurai et al. 2014a; Sakurai and Katz 2016). In the nudibranch, *Melibe leonine*,
364 there is an additional pedal swim neuron (Si4), which also has only contralateral synapses
365 (Sakurai et al. 2014a). We are aware of only one connection between ipsilateral pedal ganglion
366 neurons in any nudibranch species studied; ipsilateral Si2 was shown to elicit one-for-one EPSPs
367 in pedal efferent neurons in *Melibe* (Thompson and Watson 2005). This in contrast with
368 cerebral ganglion neurons, such as Si1 the DSIs and C2, which make both ipsilateral and
369 contralateral connections (Gunaratne et al. 2017; Katz 2009; Sakurai et al. 2014a; Sakurai and
370 Katz 2019).

371 The lack of synaptic connectivity within the pedal ganglion may extend to all gastropods
372 studied. There are reports of "non-synaptic", volume transmission in the pteropod *Clione*
373 *limacina* (Arshavsky et al. 1988) and a slow inhibitory synapse between two pedal neurons in
374 *Lymnaea stagnalis* (Inoue et al. 1996), however there are no reports of one-for-one fast
375 synaptic potentials between neurons within the pedal ganglion for any gastropod. This suggests
376 something fundamental about the organization of gastropod nervous systems, namely that
377 aside from the limited number of contralaterally-projecting interneurons, the majority of pedal
378 ganglion neurons are efferent, projecting to the rest of the body.

379 Thus, the organization of the two modules being composed of contralateral Si2 and Si3
380 may be a result of a constraint on the system. The CPG could not be composed neurons on the
381 left acting together because they do not synapse on each other. Thus, the only way to construct
382 a half-center oscillator is to have each half composed of contralateral neurons.

383 *Comparisons to the Melibe swim CPG*

384 The nudibranch, *Melibe*, swims with rhythmic left-right body flexions like *Dendronotus*. The
385 swimming behaviors are likely homologous because all species within the clade swim in this

386 manner (Sakurai and Katz 2017). The *Melibe* swim CPG, which consists of 8 neurons (left and
387 right) Si1, Si2, Si3, and Si4, is also organized into a half-center configuration, but the roles of Si2
388 and Si3 differ from those in *Dendronotus* (Sakurai et al. 2014a; Sakurai and Katz 2017; 2016;
389 Sakurai et al. 2014b). The primary half-center kernel, consists of Si1, Si2, and Si4, which can
390 generate alternating burst discharges without Si3. The role of Si3 is to terminate the bursts of
391 each module.

392 Thus, homologous neurons have opposite functions in the two HCOs; in *Dendronotus*,
393 Si3 initiates bursts and Si2 terminates them, but in *Melibe* S2 is part of the burst generator and
394 Si3 terminates the bursts. These differences arise in part due to differences in the synaptic
395 actions and connectivity of the homologous neurons. In addition, Si1, which is part of the HCO
396 in *Melibe*, plays an extrinsic neuromodulatory role in *Dendronotus*, enhancing the synaptic
397 actions of Si3 (Sakurai and Katz 2019).

398 The direction of evolutionary change is not clear. We do not know if the more complex
399 eight cell *Melibe* CPG arose from a simpler ancestral *Dendronotus*-like circuit or whether the
400 *Dendronotus* swim CPG arose as refinement of a larger *Melibe*-like circuit. Regardless of how it
401 arose, the *Dendronotus* swim CPG is beautiful in its simplicity; two neurons with
402 complementary synaptic actions and membrane properties partition the functions needed to
403 ensure stable alternating bursts.

404 **Figure Legends**

405 **Figure 1.** The central pattern generator (CPG) underlying the swimming behavior of
406 *Dendronotus iris*. ***A***. Schematic drawing of the cell body locations and the axonal projections of
407 the swim CPG neurons, Si2 (blue) and Si3 (red), in the *Dendronotus* brain, showing Cerebral,
408 Pleural, and two Pedal (proximal and distal) ganglia based on Sakurai and Katz (2016). Si2 and
409 Si3 have their cell bodies in the proximal pedal ganglion. They each project an axon to the
410 contralateral pedal ganglion through one of the two pedal commissures. Only L-Si2 and R-Si3
411 axon projections are depicted. ***B***. The previously published connectivity of the *Dendronotus*
412 swim CPG. Each module of the half-center oscillator that constitutes the swimming circuit is
413 composed of Si2 and Si3 with cell bodies on opposite sides. Module α consists of the left Si2
414 and right Si3, and module β consists of the right Si2 and left Si3. Lines terminating in triangles
415 indicate excitatory synapses, filled circles inhibitory synapses. Resistor symbols indicate
416 electrical connections. ***C***. The swim motor pattern recorded intracellularly from all four swim
417 interneurons (***Ci***). Si2 and Si3 in the same module fire bursts of action potentials together. The
418 two modules exhibit alternating bursts. A portion of the traces indicated by the dotted box is
419 enlarged in ***Cii***. L-Si3 spikes evoke EPSPs in the R-Si2, leading to one-for-one spikes.

420

421 **Figure 2.** The inhibitory synaptic potentials generated by Si2 and Si3 have different reversal
422 potentials. ***A***. Schematic diagrams of synaptic connections in the swim CPG and overlaid traces
423 of L-Si2 to R-Si2 (*Ai*) and L-Si3 to R-Si3 (*Aii*) synaptic potentials in Hi-Di saline. One electrode was
424 inserted into L-Si2 (*Ai*) or R-Si3 (*Aii*) to record the presynaptic action potentials, while two
425 electrodes (one for voltage recording and the other for current injection) inserted into R-Si2 (*Ai*)
426 or L-Si3 (*Aii*), respectively. Positive or negative current was injected into the postsynaptic cell
427 (R-Si2 or L-Si3) to change its membrane potential. The numbers on the left side of the traces
428 indicate the postsynaptic membrane potential. Ten traces were overlaid for each voltage level.
429 Traces were triggered at the peak of presynaptic action potentials. ***B***. The relationships
430 between the amplitude of the IPSPs and the membrane potential of the postsynaptic cell are

431 shown. The values used are derived from the data shown in *A*. The white circles indicate the
432 Si2-evoked IPSPSs in the contralateral Si2, and the filled circles are the Si3-evoked IPSPs in the
433 contralateral Si3. The regression lines were drawn for the linear portion only.

434

435 **Figure 3.** An Si2 spike train causes a post-inhibitory rebound discharge in Si3 of the contralateral
436 module. Top: schematic of circuit with recorded neurons highlighted. Middle: Simultaneous
437 intracellular microelectrode recordings. Bottom: Plot of instantaneous spike frequency of
438 stimulated neuron. ***A.*** Depolarization of the L-Si2 with a 4 sec, 4 nA current pulse, caused it to
439 fire spike train with a peak frequency of 15 Hz, that declined to about 10 Hz. Si2 spiking evoked
440 hyperpolarizing responses in Si2 and Si3 of the other module, followed by post-inhibitory
441 discharges in the L-Si3 that evoked EPSPs in the R-Si2 (asterisks). ***B***. Depolarization of the R-Si3
442 with a 4 sec, 3 nA current pulse caused is to fire with a peak frequency of 14 Hz, which decayed
443 to 10 Hz. Si3 spiking produced only small hyperpolarization in the neurons of the other module
444 and caused no rebound discharge.

445

446 **Figure 4.** A Si2 spike train causes a sag depolarization and a post-inhibitory rebound
447 depolarization in postsynaptic Si3. ***A***. A 4 sec, 10 Hz spike train evoked with brief current pulses
448 (10 nA, 20 msec) in the L-Si2 caused hyperpolarization of both Si2 and Si3 in Module β. After
449 the stimulation, the membrane potential of the postsynaptic Si2 slowly recovered back to the
450 resting potential, whereas Si3 showed a faster recovery and a rebound depolarization (asterisk),
451 which lasted for 10 to 15 sec. ***B***. A 10-Hz spike train in the R-Si3 caused hyperpolarization of
452 both Si2 and Si3 in Module β. The amplitude of hyperpolarization was smaller than those
453 evoked by Si2 in ***A***, and there was no rebound depolarization after the stimulus. ***C***. Amplitudes
454 of the Si2- and Si3-evoked hyperpolarization in contralateral (*c*) and ipsilateral (*i*) postsynaptic
455 neurons. Each bar represents mean±SD (N=7-15). ***D***. Amplitudes of the post-inhibitory rebound
456 depolarization. Each bar represents mean±SD (N=7-16).

457

458 **Figure 5**. Si3 but not Si2 showed sag potential and rebound depolarization. ***A***. Membrane
459 potential responses (upper traces) of Si2 (*i*) and Si3 (*ii*) to a hyperpolarizing current pulse (-4 nA
460 for 4 sec, lower trace) in normal saline. ***B***. The numbers of spikes in Si2 (black) and Si3 (gray)
461 evoked after hyperpolarizing current pulses of various amplitudes (-1, -2, -3, and -4 nA). Each
462 bar represents mean±SD (Si2, N = 9-12; Si3, N = 7-10). The asterisk indicates significant
463 difference (see text). ***C***. Overlaid membrane potential responses (upper traces) of Si2 (*i*) and Si3
464 (*ii*) to hyperpolarizing current pulses (4 sec, -1 to -4 nA, lower traces) in Hi-Di saline. The asterisk
465 indicates a depolarizing overshoot. ***D***. Amplitudes of peak rebound depolarization with respect
466 to resting membrane potential in Si2 (black) and Si3 (gray) after hyperpolarizing current
467 injections (-1 to -4 nA, 4 sec). The asterisk indicates significant difference (see text). ***E***. The
468 amplitudes of sag depolarization, measured from peak hyperpolarization to value at end of
469 pulse, in Si2 (black) and Si3 (gray) during the hyperpolarizing current injection (-1 to -4 nA, 4
470 sec). The asterisk indicates significant difference (see text).

471

472 **Figure 6.** Si3, but not Si2, exhibited a hyperpolarization-activated inward current. ***A***. Membrane
473 current responses (upper traces) and command voltage pulses (bottom traces). The membrane
474 potentials of Si2 (left) and Si3 (right) were held at -50 mV under voltage clamp and then were
475 stepped to -60, -70, -80, -90 mV). Each neuron was impaled with two electrodes (one for
476 voltage recording and the other for current injection). All voltage-clamp experiments were
477 performed in Hi-Di saline. ***B***. The amplitudes (nA, mean±SD; Si2, N=5; Si3, N = 8) of membrane
478 current are plotted against the command voltage values (mV).

479

480 **Figure 7.** A spike train in Si2 evokes a slow inhibitory synaptic potential in Si3 in the same
481 module. ***A***. An Si2 spike train inhibited ongoing spiking activity of Si3. Simultaneous intracellular
482 records of Si2 and Si3 and the injected current traces. Tonic spiking in L-Si3 was evoked by 25
483 sec, 1 nA current pulse. A 5 sec, 2nA current pulse in the R-Si2 inhibited spiking of the L-Si3. The
484 schematic on the left shows synaptic interactions between Si2 and Si3 within the module. ***B***. A

485 spike train of Si2 (upper trace) produced complex membrane potential responses of Si3 (lower
486 trace) in the same module, part of which was mediated by chemical transmitter release. Trains
487 of action potentials in R-Si2 were evoked by injecting repetitive current pulses (7-15 nA, 20
488 msec) at 2, 5, and 10 Hz. ***Bi.*** In Hi-Di saline, the R-Si2 spikes produced sharp electrotonic EPSPs
489 in L-Si3, which overrode on a slow hyperpolarizing potential. ***Bii***. Ca^{2+}-free saline blocked the
490 slow hyperpolarizing potential, leaving the electrotonic EPSPs relatively unchanged. ***Biii.***
491 Subtraction of the Bii waveform from the Bi waveform revealed the slow hyperpolarizing
492 component that was largely blocked by the Ca^{2+}-free saline. ***C***. Amplitudes of electrotonic EPSPs
493 (upper graph) and the slow hyperpolarizing potentials (slow IPSPs; lower graph) recorded in Hi-
494 Di saline (black bars) and in Ca^{2+}-free Hi-Di saline (white bars). Ca2+-free saline diminished the
495 slow IPSPs but had little effect on the electrotonic EPSPs. Bars are mean±SD.

496

497 **Figure 8.** R-Si2 evoked a slow outwardly rectifying current in L-Si3. ***A***. Example traces of the
498 synaptic currents at different holding potentials. Spike trains were evoked in R-Si2 by injecting
499 repetitive current pulses (10 nA, 20 msec) at 10 Hz. Seven traces of the Si2 spike trains are
500 overlaid and shown at the top, whereas the slow IPSPs in L-Si3, which was voltage-clamped at
501 various potential levels, are shown below. The holding potentials (from -90 mV to -30 mV) are
502 shown on the left side of the trace. ***B***. The amplitudes of the slow IPSPs plotted against the
503 holding potential of the postsynaptic Si3. ***C***. The holding current was linear with respect to the
504 holding potentials used in this voltage-clamp experiment.

505

506 **Figure 9.** Suppression of the R-Si2 spiking prolonged Si3 bursts. ***A***. Simultaneous intracellular
507 recordings of an Si2 pair and an L-Si3. A plot of instantaneous spike frequency is shown at the
508 bottom. From the time indicated by the arrow, a hyperpolarizing current of -4 nA was applied
509 to suppress the action potential firing of R-Si2. During the hyperpolarization, trains of EPSPs
510 evoked by the L-Si3 spikes are visible in R-Si2. The bursts before and during the hyperpolarizing
511 current injection are boxed by blue (a) and red (b) dotted lines. The spike frequency during the

512 period is indicated by the same color in the plot below. ***B***. A comparison of bursts before (***a*** –
513 blue) and during the hyperpolarizing current injection (***b*** –red), expanded from ***A***. The dotted
514 lines indicate 0 mV. ***C.*** Comparisons of burst duration (Ci), burst duty cycle (Cii), and the number
515 of Si3 spikes per burst (Ciii) before (blue) and immediately after (red) the suppression of the Si2
516 spikes by hyperpolarizing current injection. All three factors increased when the Si2 spikes were
517 suppressed. Mean±SD represented by filled circle and error bars.

518

519 **Figure 10.** Artificial enhancement or suppression of slow inhibitory synaptic action of Si2 onto
520 Si3 within each half-center module changed the burst period during a swim motor pattern. ***Ai***.
521 The experimental arrangement for dynamic clamp. Every time the membrane potential (V_m) of
522 Si2 surpassed a specified threshold (50% of spike height), an artificial synaptic current (I_{Stim}) was
523 calculated by the computer and injected into the contralateral Si3 to boost the existing Si2-to-
524 Si3 slow synapse (red). Traces in ***Aii*** show the change in the burst before and during the
525 application of dynamic clamp. The red arrow indicates the time of onset of dynamic clamping.
526 The red arrow indicates the time when the dynamic clamp was started. The horizontal dotted
527 lines show 0 mV. ***B***. Simultaneous intracellular recording from all four neurons shows the effect
528 of dynamic clamping (red bar). The synaptic boost caused by adding artificial synaptic
529 conductance (500 nS) with the dynamic clamp shortening the duration of bursts and decreased
530 the period. ***C***. Synaptic suppression by counteracting IPSPs with a negative postsynaptic
531 conductance to Si3 extended the burst duration and consequently increased the period. ***D***. Plot
532 of burst periods against the conductance of artificial synapses from Si2 to Si3 in the same half-
533 center module. Increasing the synaptic conductance reduced the burst period, whereas
534 counteracting it extended the burst period.

535

536 **Figure 11**. Sequence of activities of the CPG neurons. ***A***. The updated connectivity of the
537 *Dendronotus* swim CPG. In each module (α and β) Si3 makes an excitatory synapse on the
538 contralateral Si2, which returns a slow inhibitory synapse onto the Si3. Lines terminating in

539 triangles indicate excitatory synapses, filled circles inhibitory synapses. Resistor symbols
540 indicate electrical connections. ***B***. The activity of a circuit neuron is divided into four parts (**a**, **b**,
541 **c**, **d**) shown schematically in **C.** In **Phase a**, Si2 inhibition of Si3 increases, causing the firing
542 frequency of Si2 and Si3 in module β to decline, thereby decreasing inhibition of module α.
543 **Phase b**, Si3 in module α starts firing, and Si2, which is driven by Si3, begins to fire a little later.
544 **Phase c.** Si2 inhibition of Si3 increases, causing the firing frequency of Si2 and Si3 in module α
545 to decline, thereby decreasing inhibition of module β. **Phase d.** Si3 in module β escapes from
546 inhibition and starts firing together with Si2 and suppressing activity in module α.

547 **References**

548 **Arbas EA, and Calabrese RL**. Slow oscillations of membrane potential in interneurons that control
549 heartbeat in the medicinal leech. *J Neurosci* 7: 3953-3960, 1987.
550 **Arshavsky Y, I., Deliagina TG, Orlovsky GN, Panchin YV, Pavlova GA, and Popova LB**. Control of
551 locomotion in marine mollusc Clione limacina. VI. Activity of isolated neurons of pedal ganglia.
552 *Experimental brain research* 63: 106-112, 1986.
553 **Arshavsky YI, Beloozerova IN, Orlovsky GN, Panchin YV, and Pavlova GA**. Control of locomotion in
554 marine mollusc Clione limacina. III. On the origin of locomotory rhythm. *Experimental brain research* 58:
555 273-284, 1985.
556 **Arshavsky YI, Deliagina TG, Gelfand M, Orlovsky GN, Panchin YV, Pavlova GA, and Popova LB**. Non-
557 synaptic interaction between neurons in molluscs. *Comp Biochem Physiol* 91C: 199-203, 1988.
558 **Ausborn J, Snyder AC, Shevtsova NA, Rybak IA, and Rubin JE**. State-dependent rhythmogenesis and
559 frequency control in a half-center locomotor CPG. *J Neurophysiol* 119: 96-117, 2018.
560 **Brown TG**. The Intrinsic Factors in the Act of Progression in the Mammal. *Proc R Soc Lond B* 84: 308-319,
561 1911.
562 **Cymbalyuk GS, Gaudry Q, Masino MA, and Calabrese RL**. Bursting in leech heart interneurons: cell-
563 autonomous and network-based mechanisms. *J Neurosci* 22: 10580-10592, 2002.
564 **Daun S, Rubin JE, and Rybak IA**. Control of oscillation periods and phase durations in half-center central
565 pattern generators: a comparative mechanistic analysis. *Journal of computational neuroscience* 27: 3-36,
566 2009.
567 **Destexhe A, Mainen ZF, and Sejnowski TJ**. An Efficient Method for Computing Synaptic Conductances
568 Based on a Kinetic Model of Receptor Binding. *Neural Comput* 6: 14-18, 1994.
569 **Dethier J, Drion G, Franci A, and Sepulchre R**. A positive feedback at the cellular level promotes
570 robustness and modulation at the circuit level. *J Neurophysiol* 114: 2472-2484, 2015.
571 **Friesen WO**. Reciprocal inhibition: a mechanism underlying oscillatory animal movements. *Neuroscience*
572 *and biobehavioral reviews* 18: 547-553, 1994.
573 **Grillner S**. The motor infrastructure: from ion channels to neuronal networks. *Nat Rev Neurosci* 4: 573-
574 586, 2003.
575 **Grillner S, and El Manira A**. The intrinsic operation of the networks that make us locomote. *Curr Opin*
576 *Neurobiol* 31: 244-249, 2015.

577 **Gunaratne CA, Sakurai A, and Katz PS**. Variations on a theme: species differences in synaptic
578 connectivity do not predict central pattern generator activity. *J Neurophysiol* 118: 1123-1132, 2017.
579 **Hagglund M, Dougherty KJ, Borgius L, Itohara S, Iwasato T, and Kiehn O**. Optogenetic dissection reveals
580 multiple rhythmogenic modules underlying locomotion. *Proc Natl Acad Sci U S A* 110: 11589-11594,
581 2013.
582 **Inoue T, Takasaki M, Lukowiak K, and Syed N**. Inhibition of the respiratory pattern-generating neurons
583 by an identified whole-body withdrawal interneuron of Lymnaea stagnalis. *The Journal of experimental*
584 *biology* 199: 1887-1898, 1996.
585 **Jiao Y, Cao Y, Zheng Z, Liu M, and Guo X**. Massive expansion and diversity of nicotinic acetylcholine
586 receptors in lophotrochozoans. *BMC Genomics* 20: 937, 2019.
587 **Katz PS**. *Tritonia* swim network. *Scholarpedia* 4: 3638, 2009.
588 **Kemenes I, Marra V, Crossley M, Samu D, Staras K, Kemenes G, and Nowotny T**. Dynamic clamp with
589 StdpC software. *Nat Protoc* 6: 405-417, 2011.
590 **Kiehn O**. Decoding the organization of spinal circuits that control locomotion. *Nat Rev Neurosci* 17: 224-
591 238, 2016.
592 **Kiehn O, Johnson BR, and Raastad M**. Plateau properties in mammalian spinal interneurons during
593 transmitter-induced locomotor activity. *Neuroscience* 75: 263-273, 1996.
594 **Li WC, and Moult PR**. The control of locomotor frequency by excitation and inhibition. *J Neurosci* 32:
595 6220-6230, 2012.
596 **Li WC, Roberts A, and Soffe SR**. Specific brainstem neurons switch each other into pacemaker mode to
597 drive movement by activating NMDA receptors. *J Neurosci* 30: 16609-16620, 2010.
598 **Moult PR, Cottrell GA, and Li WC**. Fast silencing reveals a lost role for reciprocal inhibition in
599 locomotion. *Neuron* 77: 129-140, 2013.
600 **Paulus W, and Rothwell JC**. Membrane resistance and shunting inhibition: where biophysics meets
601 state-dependent human neurophysiology. *J Physiol* 594: 2719-2728, 2016.
602 **Perkel DH, and Mulloney B**. Motor pattern production in reciprocally inhibitory neurons exhibiting
603 postinhibitory rebound. *Science* 185: 181-183, 1974.
604 **Pirtle TJ, Willingham K, and Satterlie RA**. A hyperpolarization-activated inward current alters swim
605 frequency of the pteropod mollusk Clione limacina. *Comp Biochem Physiol A Mol Integr Physiol* 157:
606 319-327, 2010.

607 **Reith CA, and Sillar KT**. A role for slow NMDA receptor-mediated, intrinsic neuronal oscillations in the
608 control of fast fictive swimming in Xenopus laevis larvae. *Eur J Neurosci* 10: 1329-1340, 1998.
609 **Sakurai A, Gunaratne CA, and Katz PS**. Two interconnected kernels of reciprocally inhibitory
610 interneurons underlie alternating left-right swim motor pattern generation in the mollusc *Melibe*
611 *leonina*. *J Neurophysiol* 112: 1317-1328, 2014a.
612 **Sakurai A, and Katz PS**. Artificial Synaptic Rewiring Demonstrates that Distinct Neural Circuit
613 Configurations Underlie Homologous Behaviors. *Curr Biol* 27: 1721-1734 e1723, 2017.
614 **Sakurai A, and Katz PS**. The central pattern generator underlying swimming in Dendronotus iris: a
615 simple half-center network oscillator with a twist. *J Neurophysiol* 116: 1728-1742, 2016.
616 **Sakurai A, and Katz PS**. Command or obey? Homologous neurons differ in hierarchical position for the
617 generation of homologous behaviors. *J Neurosci* 2019.
618 **Sakurai A, Tamvacakis AN, and Katz PS**. Hidden synaptic differences in a neural circuit underlie
619 differential behavioral susceptibility to a neural injury. *eLife* e02598, 2014b.
620 **Selverston AI, and Miller JP**. Mechanisms underlying pattern generation in lobster stomatogastric
621 ganglion as determined by selective inactivation of identified neurons. I. Pyloric system. *J Neurophysiol*
622 44: 1102-1121, 1980.
623 **Sharp AA, Skinner FK, and Marder E**. Mechanisms of oscillation in dynamic clamp constructed two-cell
624 half-center circuits. *J Neurophysiol* 76: 867-883, 1996.
625 **Thompson S, and Watson Wr**. Central pattern generator for swimming in Melibe. *The Journal of*
626 *experimental biology* 208: 1347-1361, 2005.
627 **van Nierop P, Bertrand S, Munno DW, Gouwenberg Y, van Minnen J, Spafford JD, Syed NI, Bertrand D,**
628 **and Smit AB**. Identification and functional expression of a family of nicotinic acetylcholine receptor
629 subunits in the central nervous system of the mollusc Lymnaea stagnalis. *J Biol Chem* 281: 1680-1691,
630 2006.
631 **van Nierop P, Keramidas A, Bertrand S, van Minnen J, Gouwenberg Y, Bertrand D, and Smit AB**.
632 Identification of molluscan nicotinic acetylcholine receptor (nAChR) subunits involved in formation of
633 cation- and anion-selective nAChRs. *J Neurosci* 25: 10617-10626, 2005.
634 **Wallen P, and Grillner S**. N-methyl-D-aspartate receptor-induced, inherent oscillatory activity in neurons
635 active during fictive locomotion in the lamprey. *J Neurosci* 7: 2745-2755, 1987.
636 **Wang XJ, and Rinzel J**. Alternating and synchronous rhythms in reciprocally inhibitory model neurons.
637 *Neural Computation* 4: 84-97, 1992.

Figure 1

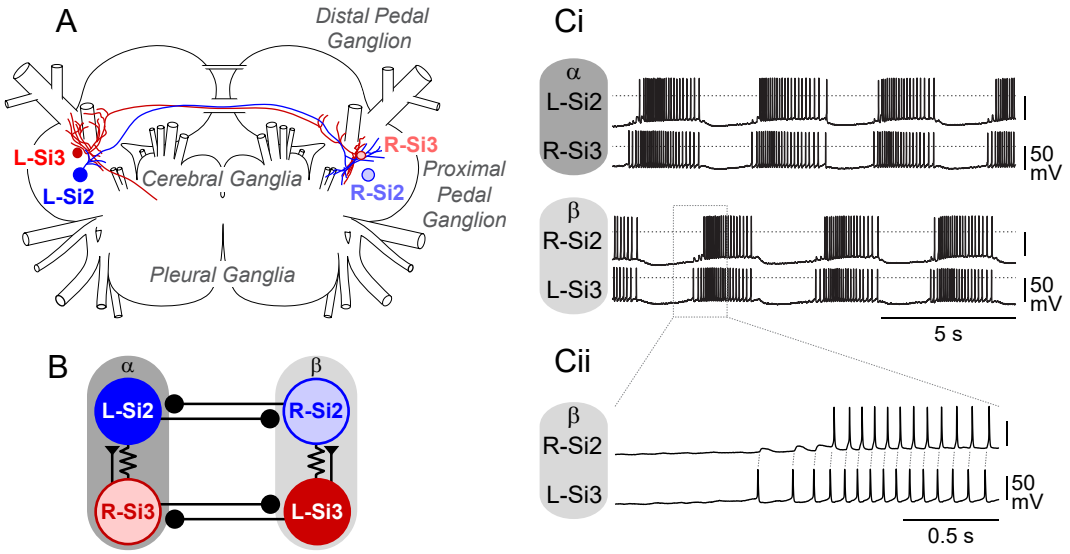

Figure 1. The central pattern generator (CPG) underlying the swimming behavior of *Dendronotus iris*. ***A***. Schematic drawing of the cell body locations and the axonal projections of the swim CPG neurons, Si2 (blue) and Si3 (red), in the *Dendronotus* brain, showing Cerebral, Pleural, and two Pedal (proximal and distal) ganglia based on Sakurai and Katz (2016). Si2 and Si3 have their cell bodies in the proximal pedal ganglion. They each project an axon to the contralateral pedal ganglion through one of the two pedal commissures. Only L-Si2 and R-Si3 axon projections are depicted. ***B***. The previously published connectivity of the *Dendronotus* swim CPG. Each module of the half-center oscillator that constitutes the swimming circuit is composed of Si2 and Si3 with cell bodies on opposite sides. Module α consists of the left Si2 and right Si3, and module β consists of the right Si2 and left Si3. Lines terminating in triangles indicate excitatory synapses, filled circles inhibitory synapses. Resistor symbols indicate electrical connections. ***C***. The swim motor pattern recorded intracellularly from all four swim interneurons (***Ci***). Si2 and Si3 in the same module fire bursts of action potentials together. The two modules exhibit alternating bursts A portion of the traces indicated by the dotted box is enlarged in ***Cii***. L-Si3 spikes evoke EPSPs in the R-Si2, leading to one-for-one spikes.

Figure 2

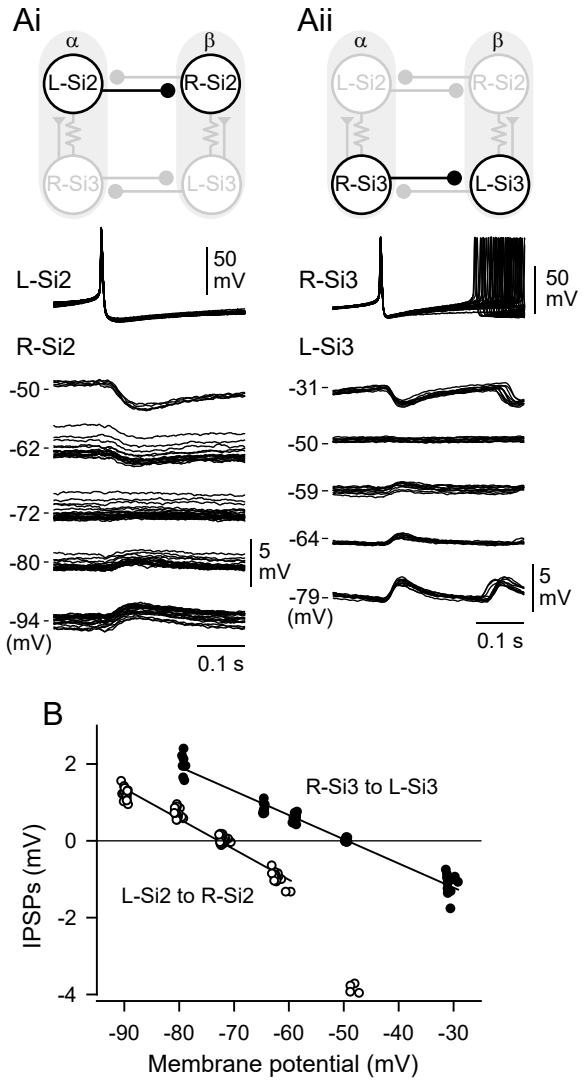

Figure 2. The inhibitory synaptic potentials generated by Si2 and Si3 have different reversal potentials. ***A***. Schematic diagrams of synaptic connections in the swim CPG and overlaid traces of L-Si2 to R-Si2 (*Ai*) and L-Si3 to R-Si3 (*Aii*) synaptic potentials in Hi-Di saline. One electrode was inserted into L-Si2 (*Ai*) or R-Si3 (*Aii*) to record the presynaptic action potentials, while two electrodes (one for voltage recording and the other for current injection) inserted into R-Si2 (*Ai*) or L-Si3 (*Aii*), respectively. Positive or negative current was injected into the postsynaptic cell (R-Si2 or L-Si3) to change its membrane potential. The numbers on the left side of the traces indicate the postsynaptic membrane potential. Ten traces were overlaid for each voltage level. Traces were triggered at the peak of presynaptic action potentials. ***B***. The relationships between the amplitude of the IPSPs and the membrane potential of the postsynaptic cell are shown. The values used are derived from the data shown in *A*. The white circles indicate the Si2-evoked IPSPSs in the contralateral Si2, and the filled circles are the Si3-evoked IPSPs in the contralateral Si3. The regression lines were drawn for the linear portion only.

Figure 3

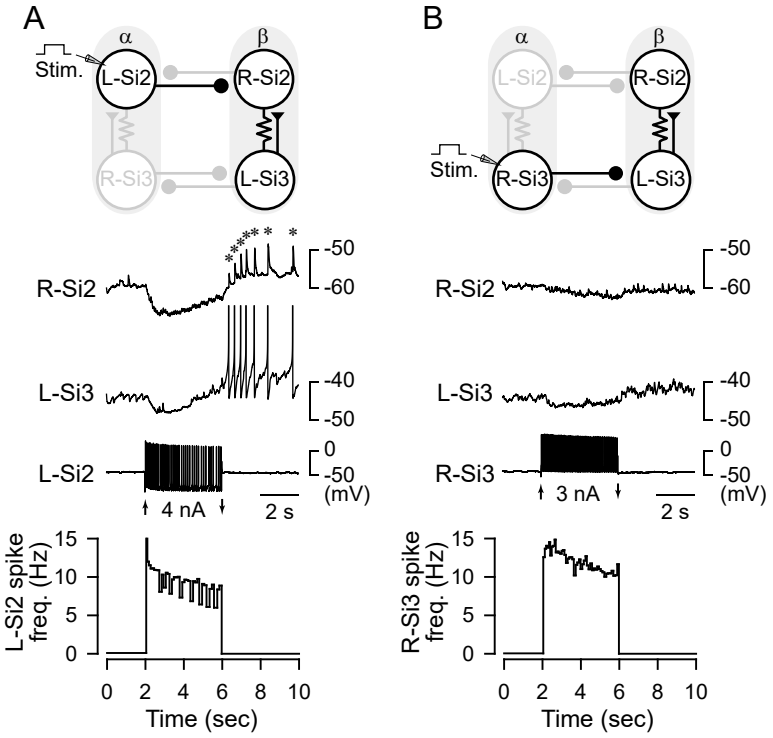

Figure 3. An Si2 spike train causes a post-inhibitory rebound discharge in Si3 of the contralateral module. Top: schematic of circuit with recorded neurons highlighted. Middle: Simultaneous intracellular microelectrode recordings. Bottom: Plot of instantaneous spike frequency of stimulated neuron. ***A.*** Depolarization of the L-Si2 with a 4 sec, 4 nA current pulse, caused it to fire spike train with a peak frequency of 15 Hz, that declined to about 10 Hz. Si2 spiking evoked hyperpolarizing responses in Si2 and Si3 of the other module, followed by post-inhibitory discharges in the L-Si3 that evoked EPSPs in the R-Si2 (asterisks). ***B***. Depolarization of the R-Si3 with a 4 sec, 3 nA current pulse caused is to fire with a peak frequency of 14 Hz, which decayed to 10 Hz. Si3 spiking produced only small hyperpolarization in the neurons of the other module and caused no rebound discharge.

Figure 4

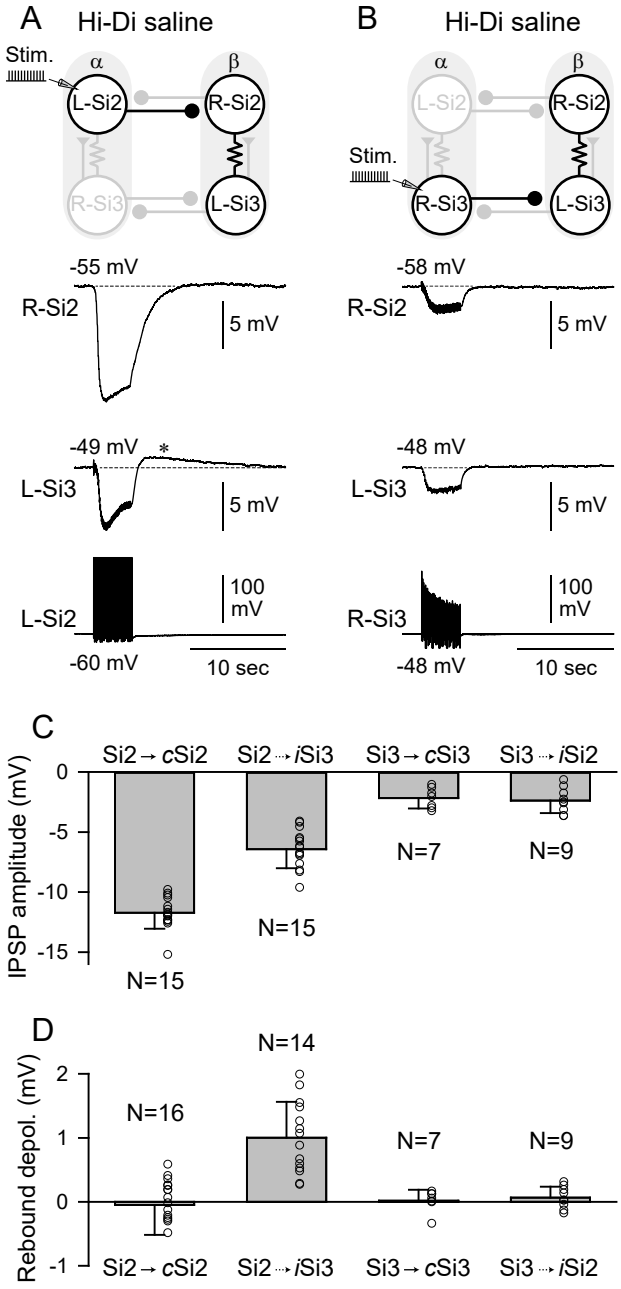

Figure 4. A Si2 spike train causes a sag depolarization and a post-inhibitory rebound depolarization in postsynaptic Si3. ***A***. A 4 sec, 10 Hz spike train evoked with brief current pulses (10 nA, 20 msec) in the L-Si2 caused hyperpolarization of both Si2 and Si3 in Module β. After the stimulation, the membrane potential of the postsynaptic Si2 slowly recovered back to the resting potential, whereas Si3 showed a faster recovery and a rebound depolarization (asterisk), which lasted for 10 to 15 sec. ***B***. A 10-Hz spike train in the R-Si3 caused hyperpolarization of both Si2 and Si3 in Module β. The amplitude of hyperpolarization was smaller than those evoked by Si2 in ***A***, and there was no rebound depolarization after the stimulus. ***C***. Amplitudes of the Si2- and Si3-evoked hyperpolarization in contralateral (*c*) and ipsilateral (*i*) postsynaptic neurons. Each bar represents mean±SD (N=7-15). ***D***. Amplitudes of the post-inhibitory rebound depolarization. Each bar represents mean±SD (N=7-16).

Figure 5

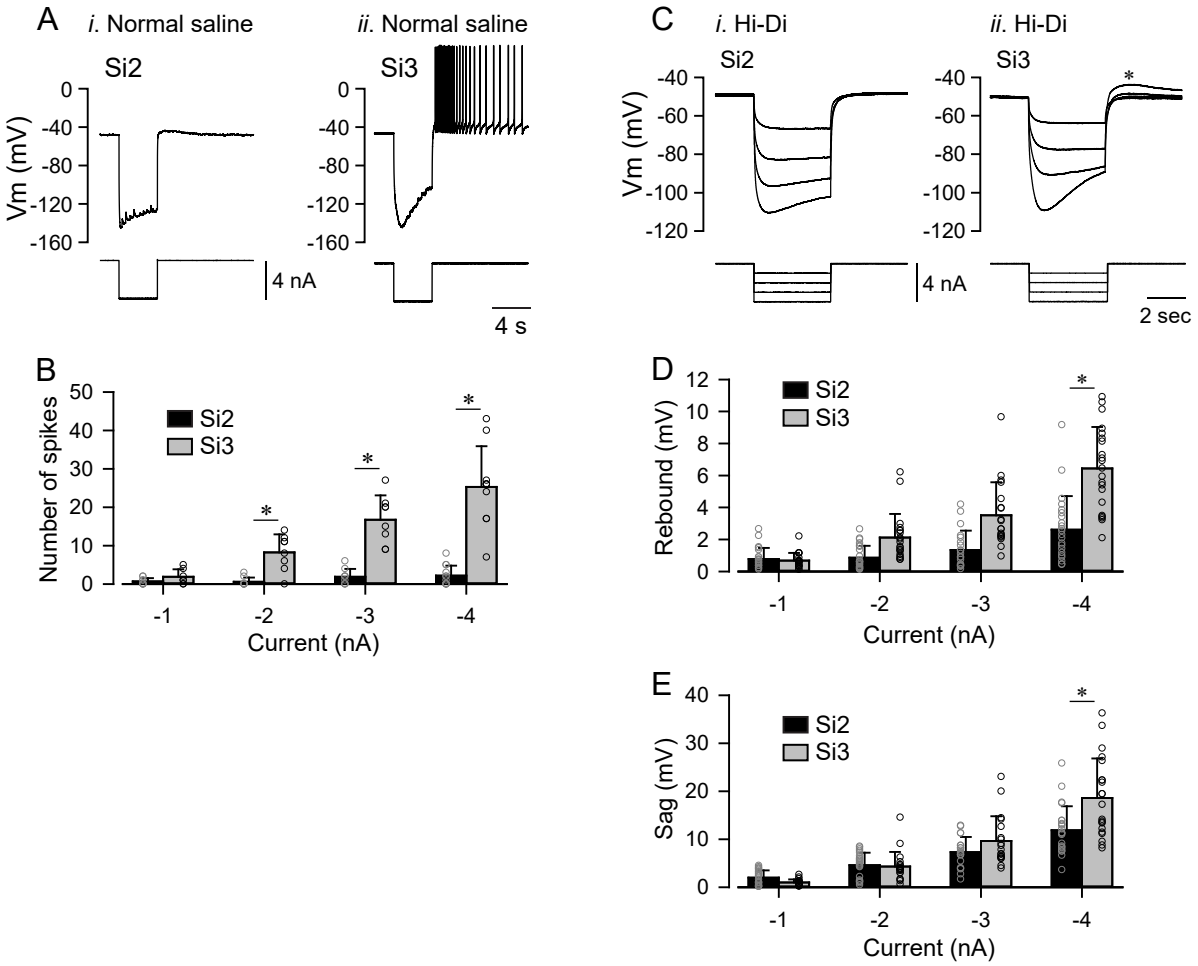

Figure 5. Si3 but not Si2 showed sag potential and rebound depolarization. ***A***. Membrane potential responses (upper traces) of Si2 (*i*) and Si3 (*ii*) to a hyperpolarizing current pulse (-4 nA for 4 sec, lower trace) in normal saline. ***B***. The numbers of spikes in Si2 (black) and Si3 (gray) evoked after hyperpolarizing current pulses of various amplitudes (-1, -2, -3, and -4 nA). Each bar represents mean±SD (Si2, N = 9-12; Si3, N = 7-10). The asterisk indicates significant difference (see text). ***C***. Overlaid membrane potential responses (upper traces) of Si2 (*i*) and Si3 (*ii*) to hyperpolarizing current pulses (4 sec, -1 to -4 nA, lower traces) in Hi-Di saline. The asterisk indicates a depolarizing overshoot. ***D***. Amplitudes of peak rebound depolarization with respect to resting membrane potential in Si2 (black) and Si3 (gray) after hyperpolarizing current injections (-1 to -4 nA, 4 sec). The asterisk indicates significant difference (see text). ***E***. The amplitudes of sag depolarization, measured from peak hyperpolarization to value at end of pulse, in Si2 (black) and Si3 (gray) during the hyperpolarizing current injection (-1 to -4 nA, 4 sec). The asterisk indicates significant difference (see text).

Figure 6

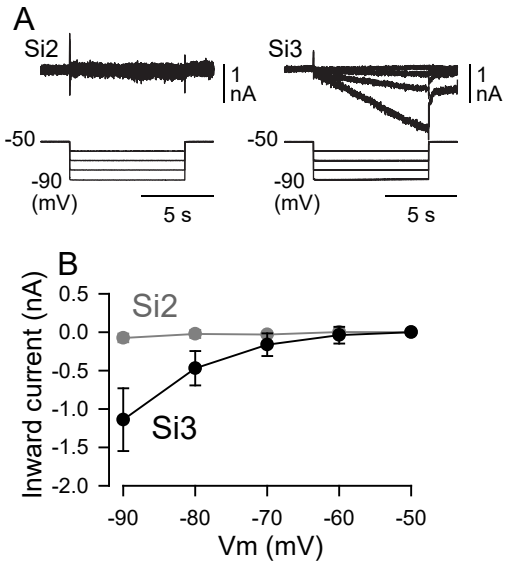

Figure 6. Si3, but not Si2, exhibited a hyperpolarization-activated inward current. ***A***. Membrane current responses (upper traces) and command voltage pulses (bottom traces). The membrane potentials of Si2 (left) and Si3 (right) were held at -50 mV under voltage clamp and then were stepped to -60, -70, -80, -90 mV). Each neuron was impaled with two electrodes (one for voltage recording and the other for current injection). All voltage-clamp experiments were performed in Hi-Di saline. ***B***. The amplitudes (nA, mean±SD; Si2, N=5; Si3, N = 8) of membrane current are plotted against the command voltage values (mV).

Figure 7

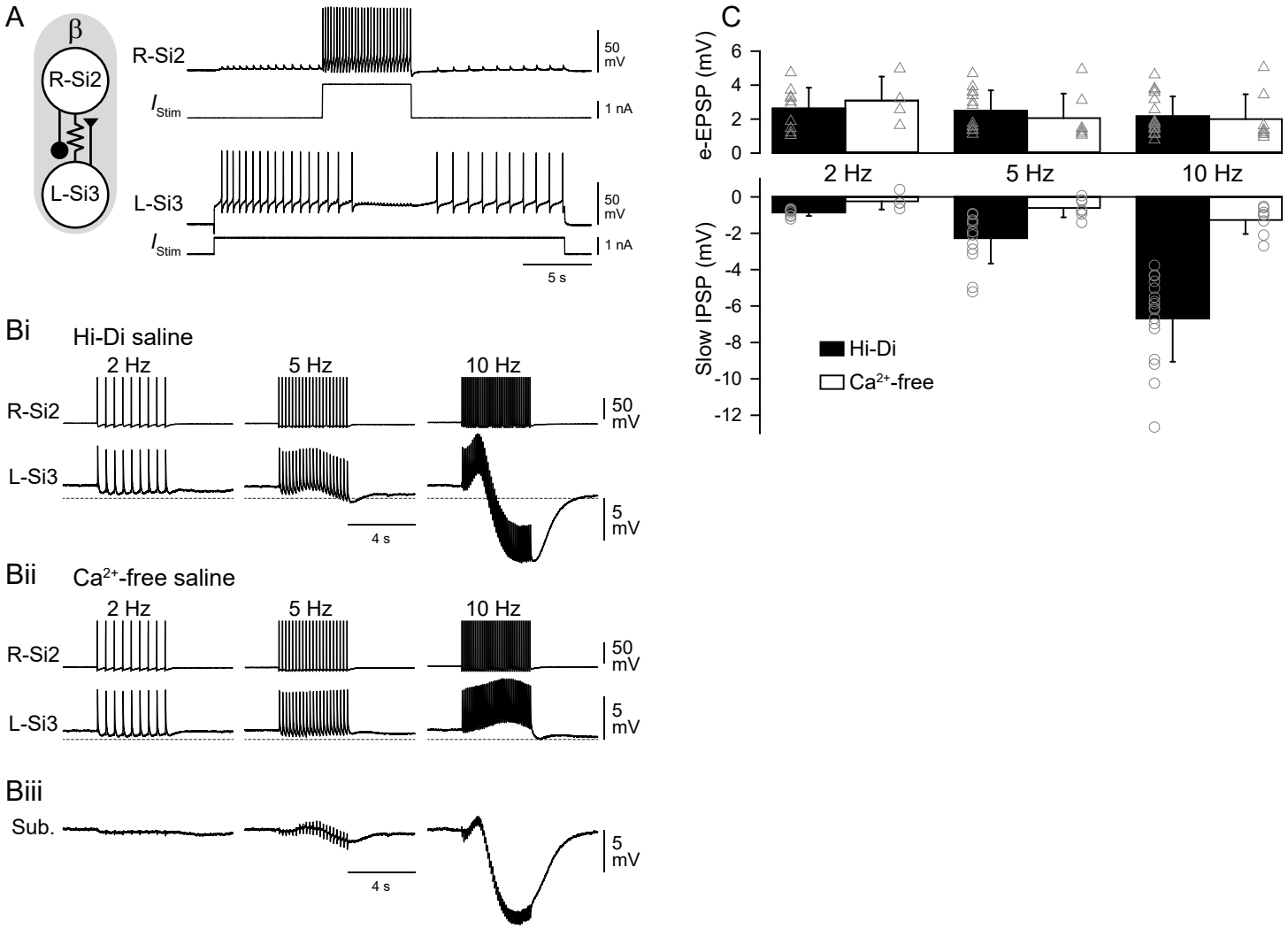

Figure 7. A spike train in Si2 evokes a slow inhibitory synaptic potential in Si3 in the same module. ***A***. An Si2 spike train inhibited ongoing spiking activity of Si3. Simultaneous intracellular records of Si2 and Si3 and the injected current traces. Tonic spiking in L-Si3 was evoked by 25 sec, 1 nA current pulse. A 5 sec, 2nA current pulse in the R-Si2 inhibited spiking of the L-Si3. The schematic on the left shows synaptic interactions between Si2 and Si3 within the module. ***B***. A spike train of Si2 (upper trace) produced complex membrane potential responses of Si3 (lower trace) in the same module, part of which was mediated by chemical transmitter release. Trains of action potentials in R-Si2 were evoked by injecting repetitive current pulses (7-15 nA, 20 msec) at 2, 5, and 10 Hz. ***Bi.*** In Hi-Di saline, the R-Si2 spikes produced sharp electrotonic EPSPs in L-Si3, which overrode on a slow hyperpolarizing potential. ***Bii***. Ca^{2+}-free saline blocked the slow hyperpolarizing potential, leaving the electrotonic EPSPs relatively unchanged. ***Biii.*** Subtraction of the Bii waveform from the Bi waveform revealed the slow hyperpolarizing component that was largely blocked by the Ca^{2+}-free saline. ***C***. Amplitudes of electrotonic EPSPs (upper graph) and the slow hyperpolarizing potentials (slow IPSPs; lower graph) recorded in Hi-Di saline (black bars) and in Ca^{2+}-free Hi-Di saline (white bars). Ca2+-free saline diminished the slow IPSPs but had little effect on the electrotonic EPSPs. Bars are mean±SD.

Figure 8

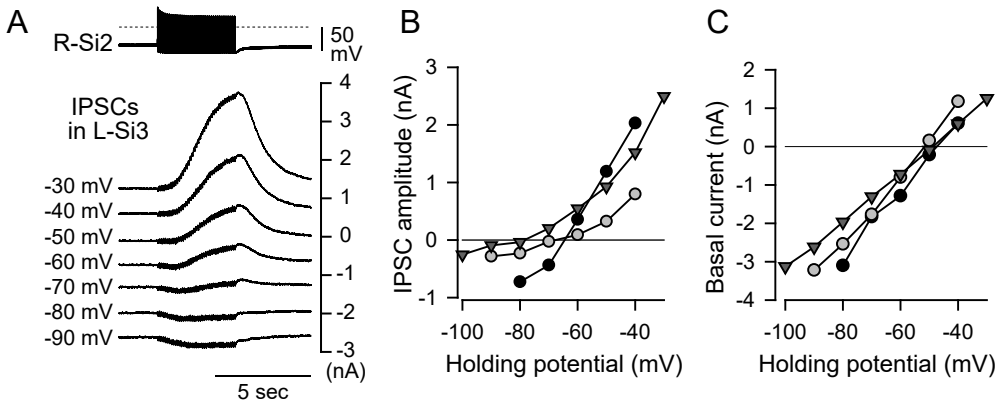

Figure 8. R-Si2 evoked a slow outwardly rectifying current in L-Si3. ***A***. Example traces of the synaptic currents at different holding potentials. Spike trains were evoked in R-Si2 by injecting repetitive current pulses (10 nA, 20 msec) at 10 Hz. Seven traces of the Si2 spike trains are overlaid and shown at the top, whereas the slow IPSPs in L-Si3, which was voltage-clamped at various potential levels, are shown below. The holding potentials (from -90 mV to -30 mV) are shown on the left side of the trace. ***B***. The amplitudes of the slow IPSPs plotted against the holding potential of the postsynaptic Si3. ***C***. The holding current was linear with respect to the holding potentials used in this voltage-clamp experiment.

Figure 9

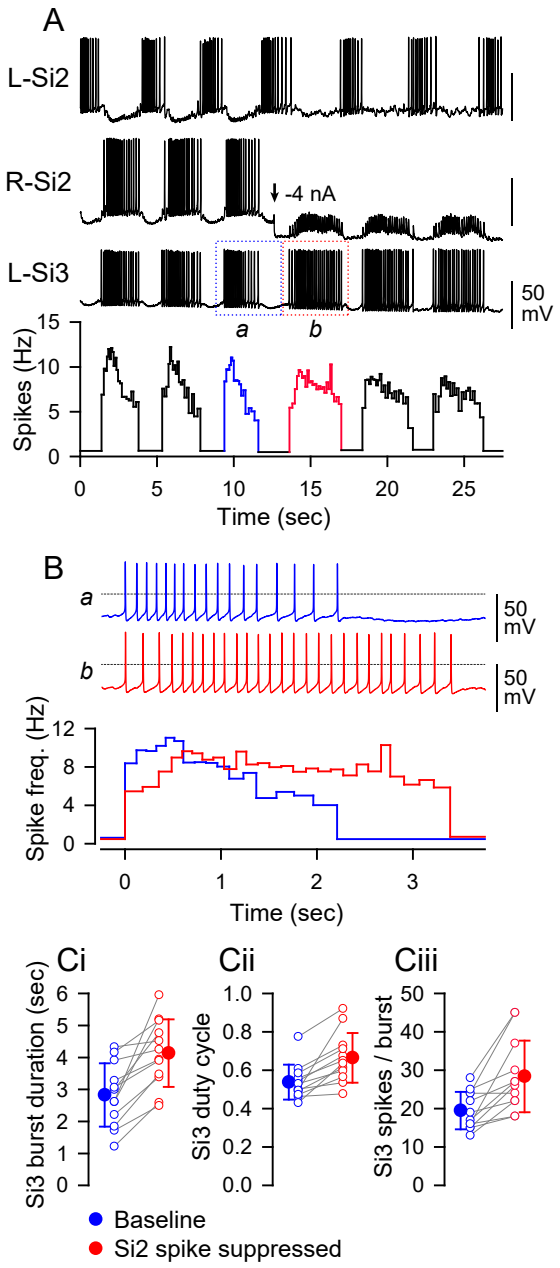

Figure 9. Suppression of the R-Si2 spiking prolonged Si3 bursts. ***A***. Simultaneous intracellular recordings of an Si2 pair and an L-Si3. A plot of instantaneous spike frequency is shown at the bottom. From the time indicated by the arrow, a hyperpolarizing current of -4 nA was applied to suppress the action potential firing of R-Si2. During the hyperpolarization, trains of EPSPs evoked by the L-Si3 spikes are visible in R-Si2. The bursts before and during the hyperpolarizing current injection are boxed by blue (a) and red (b) dotted lines. The spike frequency during the period is indicated by the same color in the plot below. ***B***. A comparison of bursts before (***a*** – blue) and during the hyperpolarizing current injection (***b*** –red), expanded from ***A***. The dotted lines indicate 0 mV. ***C.*** Comparisons of burst duration (Ci), burst duty cycle (Cii), and the number of Si3 spikes per burst (Ciii) before (blue) and immediately after (red) the suppression of the Si2 spikes by hyperpolarizing current injection. All three factors increased when the Si2 spikes were suppressed. Mean±SD represented by filled circle and error bars.

Figure 10

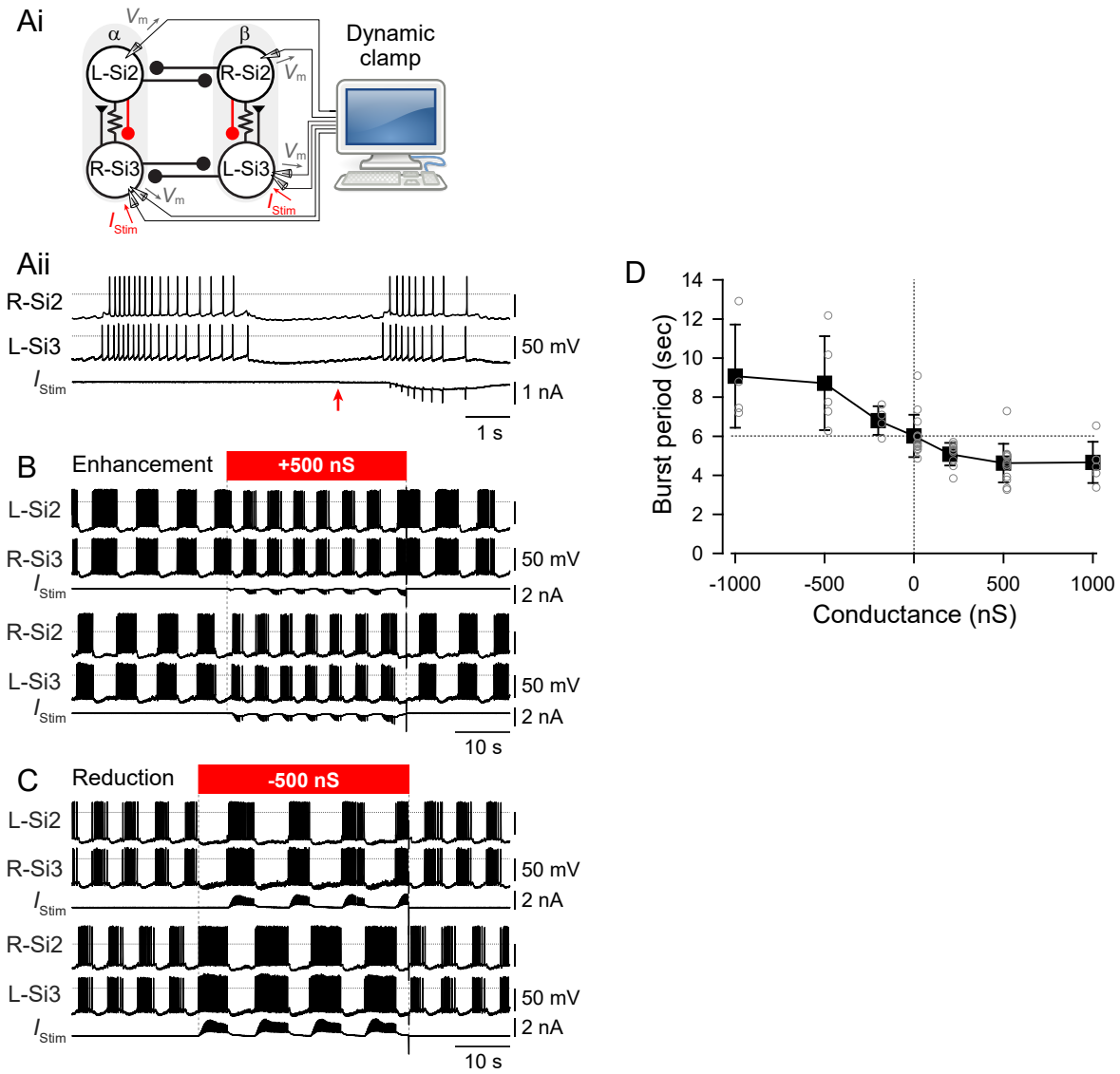

Figure 10. Artificial enhancement or suppression of slow inhibitory synaptic action of Si2 onto Si3 within each half-center module changed the burst period during a swim motor pattern. ***Ai***. The experimental arrangement for dynamic clamp. Every time the membrane potential (V_m) of Si2 surpassed a specified threshold (50% of spike height), an artificial synaptic current (I_{Stim}) was calculated by the computer and injected into the contralateral Si3 to boost the existing Si2-to-Si3 slow synapse (red). Traces in ***Aii*** show the change in the burst before and during the application of dynamic clamp. The red arrow indicates the time of onset of dynamic clamping. The red arrow indicates the time when the dynamic clamp was started. The horizontal dotted lines show 0 mV. ***B***. Simultaneous intracellular recording from all four neurons shows the effect of dynamic clamping (red bar). The synaptic boost caused by adding artificial synaptic conductance (500 nS) with the dynamic clamp shortening the duration of bursts and decreased the period. ***C***. Synaptic suppression by counteracting IPSPs with a negative postsynaptic conductance to Si3 extended the burst duration and consequently increased the period. ***D***. Plot of burst periods against the conductance of artificial synapses from Si2 to Si3 in the same half-center module. Increasing the synaptic conductance reduced the burst period, whereas counteracting it extended the burst period.

Figure 11

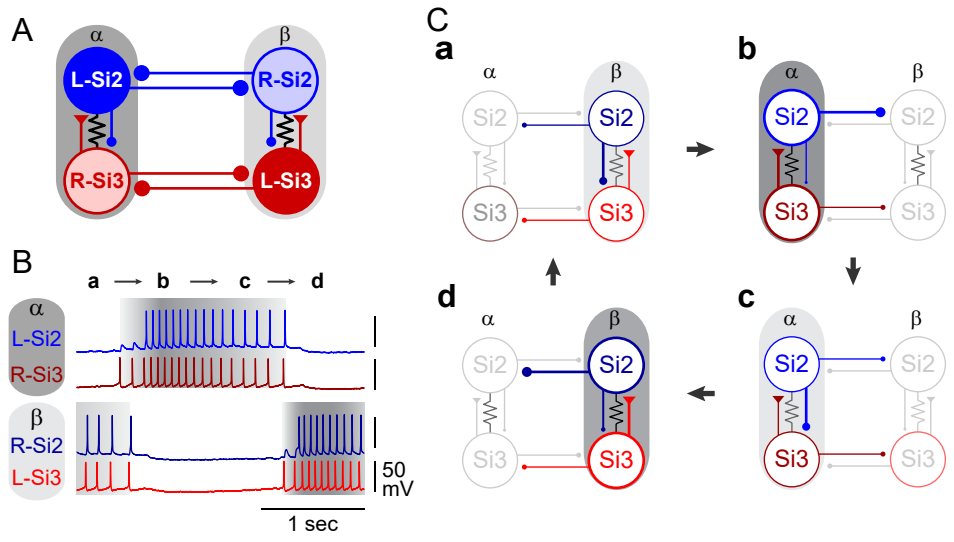

Figure 11. Sequence of activities of the CPG neurons. ***A***. The updated connectivity of the *Dendronotus* swim CPG. In each module (α and β) Si3 makes an excitatory synapse on the contralateral Si2, which returns a slow inhibitory synapse onto the Si3. Lines terminating in triangles indicate excitatory synapses, filled circles inhibitory synapses. Resistor symbols indicate electrical connections. ***B***. The activity of a circuit neuron is divided into four parts (**a**, **b**, **c**, **d**) shown schematically in **C.** In **Phase a**, Si2 inhibition of Si3 increases, causing the firing frequency of Si2 and Si3 in module β to decline, thereby decreasing inhibition of module α. **Phase b**, Si3 in module α starts firing, and Si2, which is driven by Si3, begins to fire a little later. **Phase c.** Si2 inhibition of Si3 increases, causing the firing frequency of Si2 and Si3 in module α to decline, thereby decreasing inhibition of module β. **Phase d.** Si3 in module β escapes from inhibition and starts firing together with Si2 and suppressing activity in module α.